SPECT Measurement of Benzodiazepine Receptors in Human Brain with Iodine-123-Iomazenil: Kinetic and Equilibrium Paradigms

Anissa Abi-Dargham, Marc Laruelle, John Seibyl, Zachary Rattner, Ronald M. Baldwin, Sami S. Zoghbi, Yolanda Zea-Ponce, J. Douglas Bremner, Thomas M. Hyde, Dennis S. Charney, Paul B. Hoffer and Robert B. Innis

Departments of Psychiatry and Diagnostic Radiology, Yale University School of Medicine, New Haven, Connecticut and West Haven VA Medical Center, West Haven, Connecticut; Clinical Brain Disorders Branch, IRP, NIMH Neuroscience Center at St. Elizabeths, Washington, DC

Iodine-123-iomazenil binding to benzodiazepine receptors in human brain was measured with SPECT using kinetic and equilibrium methods. **Methods:** In the kinetic experiments (n = 6), regional time-activity curves after a single bolus injection of the tracer were fit to a three-compartment model to provide estimates of the rate constants K_1 to k_4. The binding potential (equal to the product of the receptor density and affinity) was derived from the rate constants. In the equilibrium method (n = 8), the tracer bolus injection was followed by a constant tracer infusion to induce a sustained equilibrium state. The regional equilibrium volume of distribution was calculated as the ratio of the regional brain concentration-to-the free parent tracer steady-state plasma concentration. In three experiments, a receptor-saturating dose of flumazenil was injected for direct measurement of the nondisplaceable compartment distribution volume. **Results:** The kinetic and equilibrium method results were in good agreement in all regions investigated. Iodine-125-iomazenil binding potential measured in vitro in 12 postmortem samples was found to be consistent with SPECT in vivo measurements. **Conclusion:** These studies demonstrated the feasibility of quantification of receptor binding with SPECT.

Key Words: SPECT; brain; benzodiazepine receptors; Iodine-123-iomazenil

J Nucl Med 1994; 35:228–238

Alterations of central benzodiazepine receptors have been described in several neuropsychiatric conditions, including epilepsy (*1–3*), Alzheimer's disease (*4,5*), Huntington's chorea (*6–8*) and schizophrenia (*9–11*). Carbon-11-flumazenil (Ro 15-1788), a benzodiazepine antagonist, has been used as a PET radiotracer for visualization and quantification of benzodiazepine receptors in humans (*2,12–16*). Recently, an iodinated analog of flumazenil, iomazenil (Ro 16-0154), has been introduced as a SPECT radiotracer (*17*). SPECT studies in nonhuman primates (*18*) and healthy human subjects (*19*) have shown that [^{123}I]iomazenil had a high brain uptake (10%–12% of the injected dose). About 90% of this brain activity is displaceable and therefore, associated with specific binding to benzodiazepine receptors.

Analysis of SPECT neuroreceptor imaging studies have been typically restricted to empirical, semiquantitative methods such as the ratio of activities in regions of interest (ROIs) or the ROI washout rates. Since these empirical measures do not control for factors such as peripheral clearance, binding to plasma proteins and cerebral blood flow, the ability of these measures to provide quantitative information about the receptors under study is questionable (*20*). The goal of the studies reported here was to develop model-based methods for SPECT measurement of [^{123}I]iomazenil binding to benzodiazepine receptors in the human brain.

Model-based methods for in vivo quantification of neuroreceptors can be broadly divided into kinetic and equilibrium methods. Kinetic methods yield quantitative information about the receptors by estimating the rate constants which characterize the transfer between plasma, brain and receptor compartments (*21*). Equilibrium methods derive this information by analyzing the activity distribution at equilibrium, i.e., when the receptor-ligand association and dissociation rates are equal (*22*). With both approaches, the outcome measure of experiments performed at tracer doses is a unitless number, the binding potential (BP), which equals the product of the receptor density (B_{max}, nM) and affinity ($1/K_D$, nM^{-1}) (*21*). The BP is also the equilibrium distribution volume of the receptor compartment, i.e., the ratio of specific binding in the brain-to-

Received Jul. 6, 1993; revision accepted Nov. 4, 1993.
For correspondence and reprints contact: Anissa Abi-Dargham, MD, Dept. of Psychiatry, Yale University and West Haven VA Medical Center/116A2, 950 Campbell Ave., West Haven, CT 06516.

plasma level of free parent tracer at equilibrium. Benzodiazepine receptors have been measured with [^{11}C]flumazenil and PET with kinetic (*16,23,24*) and various "equilibrium" methods (*2,25–28*).

Among equilibrium methods used to measure [^{11}C]flumazenil BP, it is important to distinguish the "peak uptake" equilibrium method (*2*) and the "transient" equilibrium method (*25,27,29*). "Peak equilibrium" methods measure the BP at peak uptake of the specific binding, usually obtained by subtracting the activity in the white matter (*2*) or the pons (*26,28*) from the activity in the ROI. At peak uptake, the BP is calculated as the ratio of activity in the ROI-to-activity in a reference region. The difficulty of this method is the proper identification of peak uptake for ligands such as [^{123}I]iomazenil which exhibit a protracted plateau phase (*19*). The "transient" equilibrium method, also called quasi-equilibrium (*27*) or pseudo-equilibrium (*25*), refers to the measure of the BP when the specific-to-nonspecific ratio or the specific binding-to-plasma tracer concentration ratio becomes constant over time (i.e., when both are decreasing at the same rate). Carson et al. (*30*) proposed the term "transient" equilibrium to describe these conditions. As opposed to the peak uptake equilibrium method, the transient equilibrium methods do not satisfy the Michaelis Menten equilibrium equation and can result in an overestimation of the BP (*30*). To overcome the technical and theoretical difficulties associated with the use of equilibrium methods after single bolus injection of the tracer, we implemented in humans the constant infusion/sustained equilibrium method (*30–32*) that we previously described in baboons (*33–35*).

In the study reported here, benzodiazepine receptor BP was measured in 14 healthy subjects with [^{123}I]iomazenil and SPECT using both a kinetic (i.e., bolus only) and a sustained equilibrium (i.e., bolus plus constant infusion) paradigm. Plasma clearance of the tracer estimated from the single bolus experiments was used to design the tracer administration protocol of the bolus plus constant infusion experiments. A direct measure of the nonspecific compartment was obtained in three of the eight constant infusion experiments by injecting a receptor saturating dose of flumazenil (0.2 mg/kg) at the end of the study. In addition, the accuracy of SPECT measurements was confirmed with [^{125}I]iomazenil binding studies to postmortem human brain samples.

METHODS

Radiolabeling

Iodine-123-iomazenil and [^{125}I]iomazenil were prepared by iododestannylation of ethyl 7-(tributylstannyl)-5,6-dihydro-5-methyl-6-oxo-4*H*-imidazo[1,5-*a*][1,4]benzodiazepine-3-carboxylate with chloramine-T in methanolic acetic acid at 120°C (*36*). Radiolabeled products were purified by reversed-phase HPLC (C-18 column, 3.9 × 300 mm, 55% CH_3OH/H_2O, 0.7 ml/min; R_t 9.2 min), formulated in 5% ethanol in normal saline containing 0.1 m*M* L-ascorbic acid, pH 5–6, and filtered through a 0.2-μ membrane filter into a sterile 10-ml serum vial or sterile 10-ml syringe. The radiochemical yield of the [^{123}I]iomazenil preparations averaged 66.4% ± 8.2% (with these and subsequent data expressed as mean ± s.d., n = 14) and the radiochemical purity averaged 97.6% ± 1.7% (n = 14). The specific activity was determined by comparing the UV absorbance of the labeled product with a standard curve generated from known concentrations of nonradioactive iomazenil. The specific activity of [^{123}I]iomazenil in these preparations was found to be greater than 5000 Ci/mmole and may be estimated to be on the order of 180,000 Ci/mmole (*37*). Sterility was assured by lack of bacterial growth in two media and apyrogenicity was confirmed using the limulus amebocyte lysate (LAL) test. The specific activity of [^{125}I]iomazenil was estimated by UV detection to be 1090 Ci/mmole on the day of labeling.

Healthy Subjects

Fourteen healthy subjects (age 26 ± 6 yr, weight 75 ± 7 kg, 11 males and 2 females) were recruited for these studies. Inclusion criteria were: (1) absence of current medical conditions and (2) absence of neuropsychiatric illness, alcohol or substance use. A physical examination, EKG and routine blood and urine tests were performed in the screening procedure. All subjects gave written informed consent. Protocols were approved by the institutional human investigation committee. Subjects received potassium iodide (SSKI solution 0.6 g in the 24 hr period prior to imaging).

Data Acquisition

SPECT data were acquired with the multislice brain-dedicated CERASPECT camera (Digital Scintigraphics, Waltham, MA) (*38*). The transaxial and axial resolution in air are 7.7 and 5.9 mm FWHM, respectively (*39*). In water, the resolution is 10–12 mm in the three planes.

Four fiducial markers filled with 10 μCi of [^{99m}Tc]sodium pertechnetate were attached on both sides of the subjects's head at the level of the cantho-meatal line to control positioning of the head in the gantry before tracer injection and to identify the cantho-meatal plane during image analysis.

Single bolus experiments were performed in six subjects (age 23 ± 0.7 yr, weight 78 ± 11 kg). Iodine-123-iomazenil (12.8 ± 4.2 mCi) was injected as a single bolus over 30 sec. Scans were acquired in continuous mode every 2 min for 145 ± 5 min. Arterial blood samples (1–2 ml) were collected every 20 sec for the first 2 min with a peristaltic pump (Harvard 2501-001, South Natick, MA) and then manually at 3, 4, 6, 8, 12, 16, 20, 30, 45 and 60 min. After the first hour, samples were drawn every 30 min until the end of the experiment.

Constant infusion experiments without flumazenil displacement were performed in five subjects (age 26 ± 9 yr, weight 75 ± 4 kg). The dose was divided in a bolus of 3.89 ± 0.39 mCi followed by a constant infusion of 1.08 ± 0.12 mCi/hr (IMED pump, Jemini PC-1, San Diego, CA) given over 450 min, resulting in a bolus-to-infusion ratio of 3.61 ± 0.27 hr. Scans were acquired in continuous mode every 5 min from 250 to 450 min postinjection. In three subjects, data were also acquired from 0 to 150 min postinjection. Arterial samples were collected in a pattern similar to the single bolus experiments in the first three experiments, and every 15 min starting 2 to 4 hr postradiotracer injection in the last five experiments.

Flumazenil displacement during [^{123}I]iomazenil constant infusion was performed in three subjects (age 27 ± 2.6 yr, weight 75 ± 12 kg). The injection and acquisition protocols were similar to the previous constant infusion studies (bolus 4.1 ± 0.54 mCi, infusion 1.12 ± 0.16 mCi/hr resulting in a bolus-to-infusion ratio of

3.64 ± 0.13 hr), with the exception that a receptor-saturating dose of flumazenil (0.2 mg/kg was given at 384 min, as an intravenous infusion over 10 min (*40*).

A brain MR image was acquired in one subject on a 1.5 Tesla Signa system (General Electric Co., Milwaukee, WI). Transaxial T1-weighted, 3-mm contiguous images were obtained using a spin-echo sequence (TE 26, TR 500, FOV 24, 2 nex with a 256 × 256 matrix). MRI was performed on the same day as the SPECT experiment. Coregistration of MR and SPECT images was done relative to a set of 10 common fiducial markers filled with 20 m*M* $CuSO_4$ and approximately 10 μCi [^{99m}Tc]sodium pertechnetate (*41*). The complete datasets (32 SPECT and 45 MR images) were resliced parallel to the cantho-meatal plane.

Image Analysis

Images were reconstructed from counts set on the iodine photopeak (159 keV) with a 10% symmetric window using a Butterworth filter (cutoff = 1 cm, power factor = 10) and displayed on a 64 × 64 × 32 matrix (pixel size = 3.3 mm × 3.3 mm, slice thickness = 3.3 mm, voxel volume = 36.7 mm^3). Attenuation correction was performed assuming uniform attenuation equal to that of water (attenuation coefficient μ = 0.150 cm^2/g) within an ellipse drawn around the skull as identified by the markers. Images were reoriented so that the cantho-meatal plane, as identified by the four fiducial markers, corresponded to the transaxial plane of the dataset.

The level of highest occipital concentration was identified by inspection of the 32 images of an acquisition obtained after peak brain uptake, usually 30 min postinjection. This level was invariably located 9–10 slices above the cantho-meatal plane. A set of three slices, including one image below and one above the level of maximal occipital activity, were then summed (upper slice). Three slices were also summed at the level of the cantho-meatal plane as defined by the markers (lower slice). Seven ROIs were drawn on the coregistered MRI slices and applied to the corresponding SPECT slices from the coregistration study. The same ROIs were used, without shape or size modification, to analyze all experiments. Pontine (1 cm^2) and cerebellar ROIs (4.3 cm^2) were positioned on the lower slice. Occipital (4.0 cm^2), frontal (3.3 cm^2), temporal (2.8 cm^2), striatal (1.5 cm^2) and thalamic (0.8 cm^2) ROIs were positioned on the upper slice.

Average cpm/pixel ROI activities were measured, decay-corrected for the time of injection and expressed in μCi/cc using a calibration factor of 0.0069 μCi/cpm. This calibration factor was measured with an ^{123}I distributed source of 13.5 cm diameter (0.8 μCi/ml) acquired and reconstructed using the same protocol. The sensitivity of the camera was monitored weekly between these studies and varied by less than 5%. A ROI was also placed on one marker to assess the uniformity of the sensitivity during the experiments. No attempts were made to correct for the scatter fraction within the photopeak window nor for partial volume effects.

Arterial Plasma Analysis

Blood samples were analyzed as previously described (*42*). Extraction (ethyl acetate) was followed by reverse-phase HPLC to measure the metabolite-corrected total plasma activity ($Ca(t)$, μCi/ml). Plasma protein binding was measured by ultracentrifugation through Centrifree membrane filters (Amicon Division, W.R. Grace & Co., Danvers, MA). The binding to plasma proteins was assumed to be rapid as compared to the other processes measured in these experiments. As a consequence, the free fraction of plasma parent compound measured by ultracentrifugation (f_1 = free parent/$Ca(t)$) (*21*) was assumed to be constant for all blood samples in a single experiment.

For single bolus experiments, the measured plasma free concentration data were fit to a sum of three exponentials

$$f_1C_a(t) = \sum_{i=1}^{3} C_{0_i}e^{-\lambda i}, \qquad \text{Eq. 1}$$

where C_{0i} is the zero-time intercept (μCi/ml) of each exponential and λ_i the elimination rate constant (min^{-1}) associated with each exponential. Plasma concentration at time zero, C_0, was related to the injected dose, D (μCi), and to the initial volume of distribution of the tracer, V_{bol}(L), by

$$C_0 = \sum_{i=i}^{3} C_{0i} = \frac{D}{V_{bol}}. \qquad \text{Eq. 2}$$

The fraction of zero-time intercept associated with each exponential, f_{0i}, was calculated as

$$f_{0i} = C_{0i}/C_0, \qquad \text{Eq. 3}$$

and the clearance (C_L, liter/hr) was calculated as

$$C_L = \frac{D}{\sum_{i=1}^{3} C_{0i}/\lambda_i}. \qquad \text{Eq. 4}$$

The clearance parameters were used to derive the interpolated values of the input function to the compartment model and to estimate the bolus-to-constant infusion ratio for the constant infusion experiments.

For bolus plus constant infusion experiments, the concentration of free parent compound is given by

$$f_1C_a(t) = \sum_{i=1}^{3} C_{0_i}e^{-\lambda_i t} + C_{ss}\sum_{i=1}^{3} f_{0i}(1 - e^{-\lambda_i t}), \qquad \text{Eq. 5}$$

where C_{SS} (μCi/ml) is the free concentration at steady-state. C_{SS} is related to C_L and the rate of infusion R_0, (μCi/hr), by

$$C_{SS} = R_0/C_L. \qquad \text{Eq. 6}$$

From Equation 5, in the absence of a bolus (C_0 = 0), the time to reach steady-state is determined by the smallest exponent (λ_3), i.e., the terminal half-life ($\ln(2)/\lambda_3$). Approximately 90% of C_{SS} is reached after 3.3 half-lives. The time to reach 90% of C_{SS} can be reduced if a bolus injection is given just prior to the initiation of the constant infusion. The optimal bolus-to-hourly infusion ratio (B/I) was calculated using the kinetic parameters derived from the single bolus experiments.

Kinetic and Equilibrium Analysis

Compartmental Model. Equilibrium and kinetic analyses were performed using the same three-compartment model (Fig. 1): (1) the arterial compartment (C_a); (2) the intracerebral nondisplaceable compartment (C_2) in which the tracer can be free or nonspecifically bound; and (3) the specifically bound compartment (C_3).

Equilibration of the nonspecifically bound tracer is assumed to be rapid in comparison to the other processes so that the ratio of the free-to-the total tracer concentration in the nondisplaceable

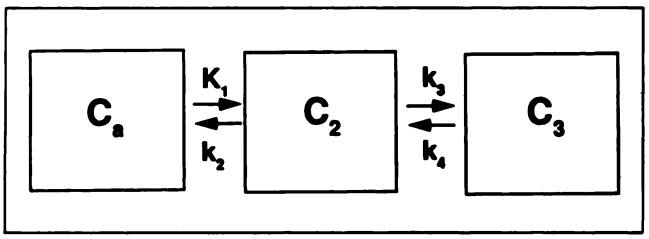

FIGURE 1. The three-compartment model used for both kinetic and equilibrium analyses. C_a = arterial plasma concentration, metabolite corrected; C_2 = tracer concentration in intracerebral nondisplaceable compartment (free and nonspecific binding); C_3 = specifically bound concentration; K_1 to k_4 = fractional rate constants describing the kinetics of tracer transfer between compartments.

compartment (f_2) is constant over time. The vascular activity present within an ROI was estimated assuming a blood volume equal to 5% of the ROI volume (*21*) and subtracted from the total ROI activity prior to analysis. The activity concentration in the ROI at time t, $C_{ROI}(t)$, is the sum of the concentrations in the second and third compartments:

$$C_{ROI}(t) = C_2(t) + C_3(t). \quad \text{Eq. 7}$$

The equilibrium volume of distribution of compartment *i* is the ratio of the tracer concentration in compartment *i* to the free tracer concentration in the arterial plasma at equilibrium, i.e., when no net transfer between the plasma and compartment *i* exists:

$$V_i = \frac{C_i}{f_1 C_a}. \quad \text{Eq. 8}$$

V_2 is the equilibrium volume of distribution of the nondisplaceable compartment and V_3 is the equilibrium distribution volume of the specifically bound compartment. The total tissue equilibrium volume of distribution, V_T, is the sum of both compartments:

$$V_T = \frac{C_{ROI}}{f_1 C_a} = V_2 + V_3. \quad \text{Eq. 9}$$

Passive diffusion is assumed to be the mechanism of transfer of the tracer across the blood-brain barrier (BBB). When the nondisplaceable compartment is at equilibrium with the plasma, the free concentration is assumed to be equal on both sides of the BBB,

$$f_1 C_a = f_2 C_2, \quad \text{Eq. 10}$$

which yields the inverse relationship between f_2 and V_2:

$$f_2 = 1/V_2. \quad \text{Eq. 11}$$

Kinetic Analysis. The tracer concentration over time in each compartment is given by:

$$\frac{dC_2(t)}{dt} = K_1 C_a(t) - k_2 C_2(t) - k_3 C_2(t) + k_4 C_3(t), \quad \text{Eq. 12}$$

$$\frac{dC_3(t)}{dt} = k_3 C_2(t) - k_4 C_3(t), \quad \text{Eq. 13}$$

where the kinetic parameters K_1 to k_4 are defined as follows:

$$K_1 = FE = F(1 - e^{-PS/F}) \quad (ml \cdot g^{-1} \cdot min^{-1}), \quad \text{Eq. 14}$$

$$k_2 = K_1/V_2 f_1 \quad (min^{-1}), \quad \text{Eq. 15}$$

$$k_3 = k_{on} B_{max} f_2 \quad (min^{-1}), \quad \text{Eq. 16}$$

$$k_4 = k_{off} \quad (min^{-1}), \quad \text{Eq. 17}$$

where F is the regional blood flow ($ml \cdot g^{-1} \cdot min^{-1}$); E the unidirectional extraction fraction; PS the permeability surface area product of the tracer ($ml \cdot g^{-1} \cdot min^{-1}$); and k_{on} and k_{off} the association and dissociation rate constants for ligand-receptor binding. Equation 15 can be derived from Equation 12 by setting k_3, k_4 and the derivates to zero and multiplying both sides by f_1.

At tracer doses, Equations 12 and 13 have constant coefficients and can be solved analytically (*43,44*), and BP can be derived from the rate constants using Equations 15, 16 and 17:

$$BP = \frac{B_{max}}{K_D} = \frac{k_{on} B_{max}}{k_{off}} = \frac{k_3}{k_4 f_2} = \frac{K_1 k_3}{k_2 k_4 f_1}. \quad \text{Eq. 18}$$

Equilibrium Analysis. At equilibrium, the rate of association and dissociation of the tracer-receptor complex are equal:

$$k_{on} f_2 C_2 B_{max} = k_{off} C_3. \quad \text{Eq. 19}$$

Thus,

$$BP = \frac{B_{max}}{K_D} = \frac{C_3}{f_2 C_2} = \frac{C_3}{f_1 C_a}, \quad \text{Eq. 20}$$

which demonstrates that BP is equal to the equilibrium volume of distribution of the bound compartment (V_3, Equation 8).

At equilibrium, V_T was calculated with Equation 9. For constant infusion experiments followed by an injection of a saturating dose of flumazenil, V_2 was calculated as the ratio of the nondisplaceable activity-to-the plasma-free parent compound (from 15 to 45 min postflumazenil injection) and BP (V_3) was calculated as the difference between V_T and V_2 (Equation 9).

Curve-Fitting Procedure. Rate constants for arterial clearance and brain uptake of the tracer were estimated by nonlinear regression using a Levenberg-Marquart least-squares minimization procedure (*45*) implemented in MATLAB (The Math Works, Inc., South Natick, MA) on a Macintosh Quadra 950. The number of exponential terms used to describe the plasma clearance was determined by the F-test (*46*) and the AIC criteria (*47*). The standard error of the parameters was given by the diagonal of the covariance matrix (*48*) and expressed as percent of the parameters (coefficient of variation, %CV). Thus, %CV indicates the identifiability of the parameter by the least-squares procedure and should not be confused with the standard deviation (s.d.) of the distribution of the parameter among subjects.

In Vitro [^{125}I]Iomazenil Binding Experiments

Twelve brains were collected from the District of Columbia Medical Examiner's Office. The brains were examined by a forensic pathologist or a neuropathologist for the detection of gross abnormalities and were cut into 1-cm thick coronal slices. Samples were dissected on ice and immediately frozen at −70°C until assayed. Inclusion criteria were absence of gross pathological abnormalities on examination of the brain and absence of neuropsychiatric disorders as noted by review of the medical records. Ages varied from 22 to 87 yr (50 ± 22 yr). Brains from four

females and eight males were used. Time between death and freezing of tissue was 24 ± 10 hr. Preservation time at −80°C was 76 ± 12 mo.

On the day of the assay, brain samples were weighed, thawed and homogenized with a Polytron (setting 6 for 10 sec) in 1/40 wet weight in mg/vol in ml (w/v) of buffer (25 m*M* KH_2PO_4, 150 m*M* NaCl, pH 7.4). After homogenization, tissues were centrifuged (20,000 g, 4°C, 10 min). The supernatant was discarded and pellets were resuspended and recentrifuged. This procedure was repeated twice. Incubation (22°C, 45 min) was initiated by the successive addition of 100 μl of [^{125}I]iomazenil, 100 μl of buffer or unlabeled iomazenil and 800 μl of tissue solution. A final tissue dilution of 1/2,400 w/v was selected so that total binding was between 5% and 10% of total ligand concentration. Incubation was terminated by rapid filtration though GF/B filters on a 48-channel Cell Harvester (Brandel, Gaithersburg, MD). Filters were rapidly washed three times with 5 ml of ice-cold buffer and counted in a COBRA 5010 gamma counter (Packard, Meriden, CT) with an efficiency of 80%. Saturation experiments (n = 12) were performed by the isotopic dilution method ("cold" saturation) on the occipital cortex from each brain using one concentration of [^{125}I]iomazenil (0.02 n*M*) and 15 concentrations of unlabeled iomazenil ranging from 10^{-14} to 10^{-6} *M*. Saturation experiments were analyzed by weighted nonlinear regression analysis using the program LIGAND (NIH, Bethesda, MD) (*49*).

RESULTS

Single Bolus Experiments

After single bolus injection of [^{123}I]iomazenil, the six subjects exhibited similar kinetics of plasma clearance of the parent compound (Table 1). In all cases, a sum of three exponentials provided a statistically significant improvement in the fit as compared to a two-exponential fit. A four-exponential fit provided a statistically significant improvement of the fit in only two of six subjects. Therefore, a three-exponential model was chosen (Fig. 2A). Initial volume of distribution was 0.44 ± 0.14 liter/kg and clearance was 7.4 ± 1.1 liter/hr/kg. The average λ_3 (0.013 ± 0.01 min^{-1}) corresponded to a terminal half-life of 97 min. The free fraction of the parent compound was between 20% and 30% of the total parent compound (f_1 = 0.23 ± 0.02).

The occipital region showed the highest and latest uptake, peaking at about 30 min (Fig. 2B). Other investigated

TABLE 1
Peripheral Clearance Parameters in Single-Bolus Experiments

Subject no.	V_{bol} (liter/kg)	C_L (liter/hr/kg)	f_1
1	0.29	6.8	0.22
2	0.52	8.2	0.23
3	0.48	7.3	0.23
4	0.41	8.5	0.23
5	0.29	5.6	0.27
6	0.64	8.4	0.21
Mean±s.d.	0.44 ± 0.14	7.4 ± 1.1	0.23 ± 0.02

V_{bol} = initial volume of distribution in plasma; C_L = peripheral clearance; and f_1 = free fraction in plasma.

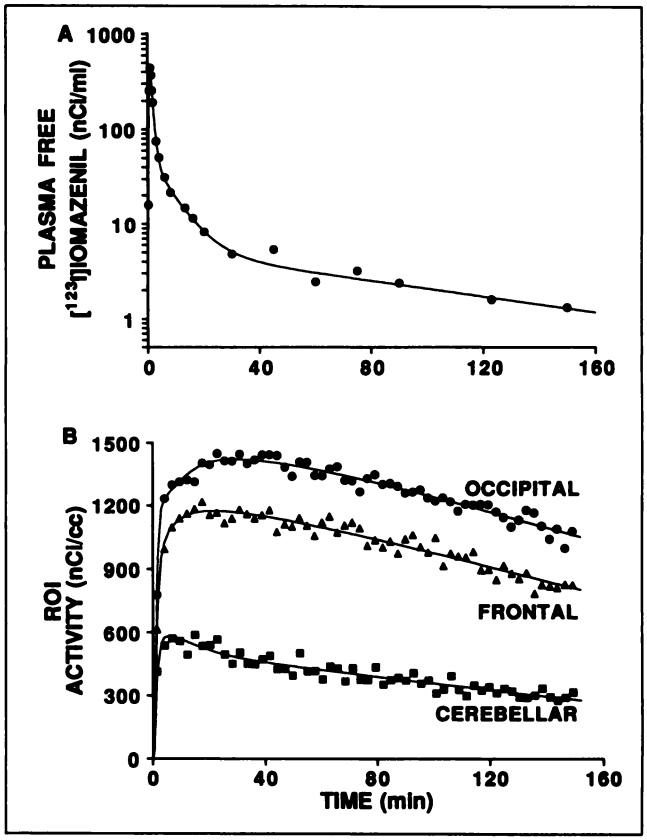

FIGURE 2. (A) Arterial time-activity curve of free parent [^{123}I]iomazenil following a bolus injection of 12.5 mCi in a 22-yr-old male. Values were fit to a triexponential model (solid line) to derive the peripheral clearance (Cl = 8.5 liter/hr/kg). (B) Regional brain time-activity curves from the same subject as in panel A. Measured values (circles, triangles and squares) were fit to a three-compartment model (solid lines). BP values were 272, 174 and 58 in the occipital cortex, frontal cortex and cerebellum, respectively.

ROIs peaked earlier and at lower values (in decreasing order temporal > frontal > striatum, thalamus, cerebellum > pons). ROI time-activity curves were fit to the three-compartment model (Fig. 2B). The iteration procedure converged for all regions, providing estimates of the regional rate constants (K_1 to k_4) and values for the outcome measures (V_2, f_2, BP and V_T, Table 2).

K_1 ranged from 0.385 ml · g^{-1} · min^{-1} (pons) to 0.546 ml · g^{-1} · min^{-1} (occipital), with an average value for all regions of 0.467 ml · g^{-1} · min^{-1}. This parameter was reasonably identified in the frontal, occipital, temporal and cerebellar regions (%CV between 5% and 6%) but was less well identified in the striatum (%CV ± s.d.; 16% ± 9%), thalamus (%CV ± s.d.; 18% ± 15%) and pons (%CV ± s.d.; 19% ± 7%). The rate constant k_2 showed a large variation across regions, from 0.094 ± 0.118 min^{-1} (temporal) to 0.300 ± 0.214 (pons) with a mean regional value of 0.151 ± 0.150 min^{-1}, and was poorly identified in all regions, with %CV ranging from 26.6% ± 8.9% in the thalamus to 127% ± 159% in the striatum. The value of k_3 varied from 0.175 ± 0.095 min^{-1} (occipital) to 0.104 ± 0.037 min^{-1} (cerebellum) but was as poorly identifiable as

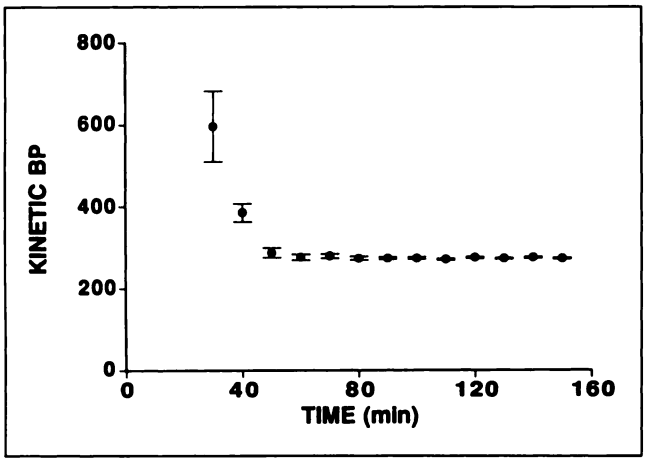

FIGURE 3. Binding potential versus length of data analysis. Following bolus injection of 12.5 mCi of [^{123}I]iomazenil, the plasma and brain data from Subject 3 were analyzed using the complete dataset acquired over 155 min and for variably shorter intervals from time 0 to that indicated on the x-axis. Values represent the kinetically derived BP ± s.e.e. These results show that BP would have been overestimated if the scanning session had been less than 60 min and reached 100% of the value determined from the complete study by 80 min.

k_2, with %CV ranging from 23.9 ± 7.3 in the cerebellum to 142% ± 84% in the thalamus. The rank order of k_3 was: occipital > frontal = striatum > thalamus > pons > temporal = cerebellum. Values of k_4 were low in all regions (regional average = 0.022 ± 0.009 min^{-1}, corresponding to a dissociation half-life of 31 min). Identifiability was better than k_2 and k_3 but worse than K_1 (with %CV ranging from 9.5% ± 2.9% in the cerebellum to 55% ± 30% in the thalamus).

BP values were significantly different among regions (occipital, 240 ± 41; temporal, 189 ± 3; frontal, 161 ± 15; cerebellum, 101 ± 23; striatum, 81 ± 12; thalamus, 78 ± 27; pons, 30 ± 11; ANOVA: $p < 0.001$), and %CV of regional means varied from 36% in the pons to 2% in the temporal. V_T also exhibited significant regional differences (ANOVA: $p < 0.001$), with %CV ranging from 8% in frontal to 30% in pons. No statistically significant regional differences in V_2 were observed (ANOVA, $p = 0.17$). V_2 regional average was 31 ± 15. The kinetic analysis estimated the average regional nonspecific binding at 20% ± 7% of the total activity. The extravascular free fraction represented 7% ± 4% of the nondisplaceable compartment.

The minimal duration of scanning needed to derive stable BP values was evaluated by fitting the occipital ROIs for various periods of time ranging from 0–50 to 0–150 min, with 20-min incremental steps (Fig. 3). In the majority of cases, the program did not converge for less than 80 min and when it did, BP values were markedly overestimated. After 80 min, BP values were within 5% of that derived by fitting the entire experiment (0–150 min).

Estimation of the Optimal Bolus-to-Infusion Ratio for Constant Infusion Experiments

Simulations were performed to estimate the optimal bolus-to-hourly infusion ratio needed to reach equilibrium rapidly in all ROIs. The system was considered at equilibrium if both plasma and brain activity were within 5% of the asymptotic equilibrium values (C_{SS} in plasma and V_T in brain). Simulations were based on the average clearance parameters and brain rate constants derived from the bolus only experiments (n = 6, Tables 1 and 2). The first simulation (mean clearance) was performed using the mean values of the group (7.4 liter/hr/kg for a 70-kg subject, λ_3 = 0.013 min^{-1}). Additional simulations were performed with clearance values corresponding to 2 s.d. below (slow clearance) and 2 s.d. above (fast clearance) the average clearance of the sampled group (398 liter/hr and 708 liter/hr, respectively). These scenarios were implemented with the corresponding λ_3 values of 0.007 and 0.022 min^{-1} for slow and fast clearance simulations, respectively. Simulations were performed for two ROIs with high (occipital, BP = 215, V_T = 233) and low (cerebellum, BP = 91, V_T = 108) densities of receptors.

For each of the three clearance conditions, time-activity curves were projected in the plasma, occipital and cerebellar ROIs for various bolus-to-hourly infusion ratios ranging from 1 to 5. Bolus-to-hourly infusion ratios between 3.2 and 4.0 fulfilled the equilibrium criteria in both ROIs in all three situations. For example, with a ratio of 3.4, the value of plasma-free parent activity integrated between 300 and 420 min was 101%, 103% and 100% of C_{SS} for the control, slow clearance and fast clearance simulation, respectively (Fig. 4A). The occipital total volume of distribution integrated during the same period was 102%, 98% and 103% of V_T for control, slow and fast clearance, respectively. In the cerebellum, the corresponding values were 105%, 102% and 104% (Fig. 4B). Thus, based on these simulations, equilibrium should be attained by 300–420 min in all ROIs, with bolus-to-infusion ratios of 3.4:4. The average bolus-to-infusion ratio used in the experiments reported here was 3.63 ± 0.21 (n = 8).

Bolus Plus Constant Infusion Experiments

In the experiment depicted in Figure 5A, arterial samples were collected from 0 to 450 min and plasma values were fit according to Equation 5. Parameters estimated from the regression were: λ_1 = 1.17; λ_2 = 0.137; λ_3 = 0.0246; f_{01} = 1.5; f_{02} = 0.0824; f_{03} = 0.0560; the clearance was estimated as 6.7 liter/hr/kg and the C_{SS} was estimated as 2.1 nCi/ml. The C_{SS} obtained by averaging the last four values (over the last hour of the experiment), 2.2 nCi/ml was fairly close to the C_{SS} estimated by the regression. Measured activities in three representative ROIs (occipital, temporal and cerebellum) from this experiment are shown in Figure 5B. SPECT data were acquired from 0 to 150 min and from 250 to 420 min. Plasma and ROI activity were stable from 180 min until the end of the infusion (420 min). Similar observations were made in two additional experi-

TABLE 2
Kinetic Analysis of Single Bolus Experiments

Parameters	Frontal	Occipital	Temporal	Striatum	Thalamus	Cerebellum	Pons
K_1 (ml · g^{-1} · min^{-1})	0.463	0.546	0.495	0.446	0.534	0.398	0.385
± s.d.	0.219	0.167	0.222	0.200	0.355	0.171	0.172
k_2 (min^{-1})	0.156	0.136	0.094	0.123	0.143	0.106	0.300
± s.d.	0.194	0.098	0.118	0.134	0.212	0.080	0.214
k_3 (min^{-1})	0.145	0.175	0.108	0.134	0.118	0.104	0.114
± s.d.	0.154	0.095	0.061	0.080	0.133	0.037	0.064
k_4 (min^{-1})	0.017	0.014	0.017	0.034	0.029	0.018	0.024
± s.d.	0.005	0.004	0.006	0.027	0.010	0.004	0.008
BP	161.00	240.00	189.00	81.00	78.00	101.00	30.00
± s.d.	15.00	41.00	3.00	12.00	27.00	23.00	11.00
f_2	0.07	0.05	0.04	0.05	0.05	0.06	0.17
± s.d.	0.09	0.03	0.03	0.03	0.04	0.03	0.09
V_2	37.00	31.00	54.00	27.00	41.00	20.00	8.00
± s.d.	25.00	30.00	54.00	19.00	30.00	11.00	4.00
V_T	198.00	271.00	242.00	108.00	119.00	121.00	37.00
± s.d.	16.00	29.00	55.00	18.00	34.00	31.00	11.00
% NSB	18.00	11.00	19.00	24.00	33.00	16.00	22.00
± s.d.	12.00	11.00	15.00	13.00	20.00	6.00	13.00

Values are mean ± s.d. of six experiments.

K_1 to k_4 = transfer rate constants; BP = binding potential as derived from kinetic analysis; f_2 = free fraction in the nondisplaceable compartment; V_2 = nondisplaceable equilibrium volume of distribution; V_T = total tissue equilibrium volume of distribution; and % NSB = percent nonspecific binding.

ments. Therefore, in subsequent experiments, arterial plasma samples and scan data were acquired only from 250 to 450 min.

To quantify the stability of the plasma and brain uptake, a linear regression was performed on plasma values (last 4 hr, mean number of points = 12) and on ROI values (last 2 hr of the experiment, mean number of points = 22). In the plasma, the mean change was 2.5% ± 2.1%/hr. With the exception of the pons, all ROIs showed changes of less than 5%/hr.

Regional V_T was measured by calculating the ratio of the averaged ROI activity and the free unmetabolized plasma activity over the last 2 hr (Table 3).

Bolus Plus Infusion Plus Displacement Experiments

Flumazenil injection was well tolerated by all three subjects with no side effects reported at the dose of 0.2 mg/kg. Flumazenil induced 88% displacement of the tracer in the occipital, 87% in the temporal, 86% in the frontal, 84% in the thalamic and cerebellar, 81% in the striatal and 60% in the pontine ROIs (n = 3). Plasma tracer activity exhibited a slight (11% ± 3%) and transient (5–15 min) increase after flumazenil injection. At the time of the measurement of V_2, the plasma tracer concentration was back to baseline. Regional V_2 varied from 34 (occipital) to 23 (pons, striatum and thalamus; Table 3 and Fig. 6). The value of f_2, calculated as $1/V_2$, varied from 0.043 (pons) to 0.030 (occipital and temporal). An important observation was the presence of 60% displaceable binding in the pons, indicating that the pons cannot be used as an area devoid of benzodiazepine receptors sites.

In Vitro [^{125}I]Iomazenil Binding in Postmortem Human Brain

In the occipital cortex, [^{125}I]iomazenil B_{max} was 162 ± 52 n*M* and K_D was 0.59 ± 0.14 n*M* (n = 12). These values corresponded to a BP of 287 ± 95. No significant correlation was observed between age and [^{125}I]iomazenil B_{max} or K_D.

DISCUSSION

These studies demonstrated the feasibility of measuring benzodiazepine receptors regional binding potential with SPECT. Two methods were tested: kinetic analysis of a single bolus injection and equilibrium analysis of bolus plus constant infusion. With the exception of the pons (where the low level of counts may have contributed to a higher level of noise), both methods gave similar regional results. For example, the occipital BP was 240 ± 41 (n = 5) and 248 ± 53 (n = 3) for kinetic and equilibrium experiments, respectively, and very close to the in vitro homogenate binding value of 287 ± 95.

The three-compartment kinetic analysis applied here was comparable to the kinetic analysis developed for reversible PET tracers such as [^{11}C]flumazenil (*16,24*). As previously observed with PET, the rate constants K_1 to k_4 were poorly identified (high standard errors due to covariance) when unconstrained kinetic analysis was applied (*30,44*). Furthermore, the values of the kinetic parameters were inconsistent with their physiological interpretation. Regional differences in K_1 and k_2 should reflect regional differences in blood flow. Their ratio, V_2 should reflect the

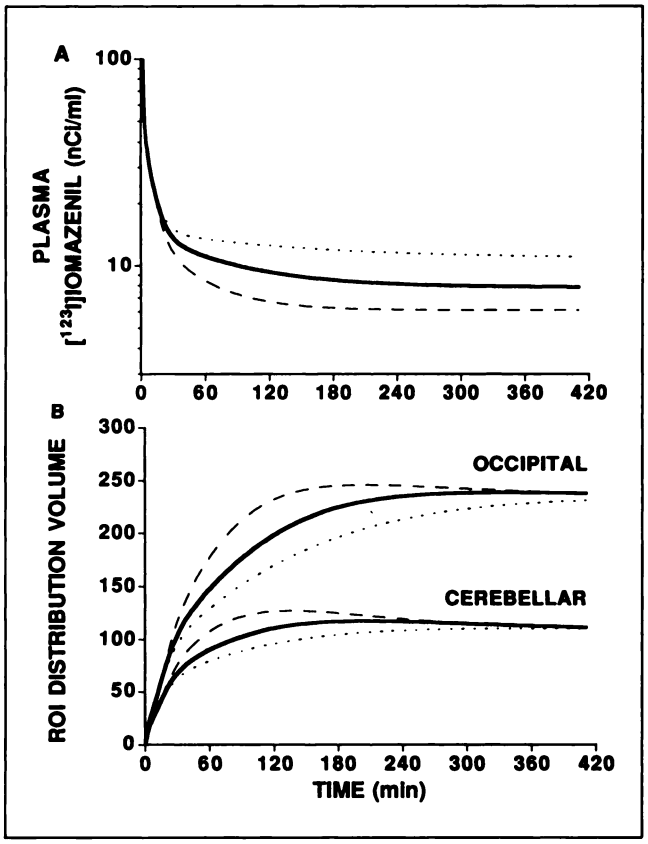

FIGURE 4. (A) Simulated plasma free [^{123}I]iomazenil concentration after a bolus injection of 3.4 mCi followed by a constant infusion of 1 mCi/hr for 420 min. The solid line represents the projected time-activity curve in a 70-kg subject with [^{123}I]iomazenil clearance of 553 liter/hr (= average clearance measured in six subjects). The dotted line (. . . .) and the broken line (– – –) are projected activities in subjects with slow (398 liter/hr) and high (708 liter/hr) clearance, respectively. In all cases, steady-state is achieved at 300 min. Simulations were generated using the following parameters: V_{bol} = 34 liter; f_{01} = 1.0; f_{02} = 0.11; f_{03} = 0.026; λ_1 = 1.18 min^{-1}; λ_2 = 0.127 min^{-1}; λ_3 = 0.013 min^{-1}, 0.007 min^{-1} and 0.022 min^{-1} in mean, slow and fast clearance scenarios, respectively. (B) Simulated volumes of distribution (regional activity/free plasma activity) in the occipital cortex and cerebellum. In both regions and in all three clearance scenarios, the volume of distribution reached an equilibrium value (V_T) at 360 min. Parameters used for this simulation were: f_1 = 0.231; K_1 = 0.546 ml · min^{-1} · g^{-1}; k_2 = 0.136 min^{-1}; k_3 = 0.175 min^{-1} (occipital) and 0.104 min^{-1} (cerebellum), k_4 = 0.0141 min^{-1}; V_2 = 17; BP = 215 (occipital), 91 (cerebellum).

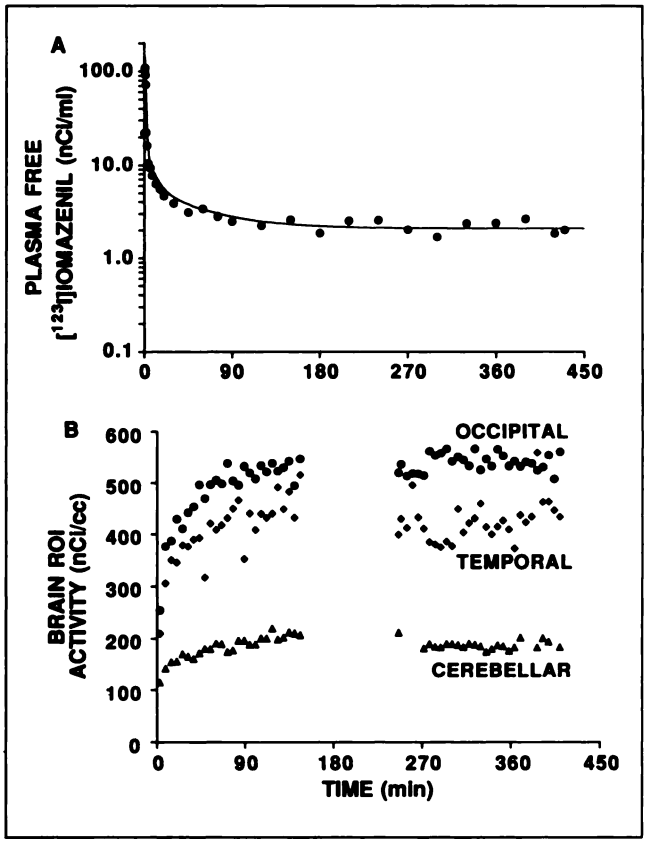

FIGURE 5. (A) Arterial time-activity curve of free unmetabolized [^{123}I]iomazenil after a bolus of 3.68 mCi followed by a constant infusion of 1.12 mCi/hr (B/I ratio of 3.68 hr) in a 21-yr-old male. Values were fit to a triexponential model (solid line) to derive the peripheral clearance (Cl = 6.7 liter/hr/kg). (B) Regional ROI time-activity curves. Total ROI activity at equilibrium (average of the last 180 min) was 0.61 μCi/ml in the occipital cortex, 0.54 μCi/ml in the temporal cortex and 0.19 μCi/ml in the cerebellum. The average level of free parent radiotracer in plasma (2.2 nCi/ml) during the last 2 hr was assumed to be equal to the free radiotracer in the brain. The ratio of total brain activity to the free gave V_T values of 276, 242 and 89 in occipital, temporal and cerebellar ROIs, respectively.

nonspecific distribution volume and is not expected to vary much between regions. In fact, V_2, as derived from kinetic analysis (Table 2), showed more regional variation than V_2 as measured directly by flumazenil displacement (Table 3). According to the model, k_3 is the parameter that includes the receptor density (B_{max}, Equation 16), leading theoretically to a correlation between V_T and k_3. No such correlation was observed (Table 2). The molecular dissociation constant, k_4 (k_{off}) is expected to be similar across regions, which was not the case (Table 2). Thus, the rate constants did not reflect the physiological processes ascribed to them by the model. However, the regional distribution of the outcome measure V_T was better identified and in accordance with the known distribution of BDZ receptors in human brain (*50–52*).

A similar situation is observed in plasma. Whereas it is unclear if a defined physiological process is associated with each exponential, the overall outcome measure, the clearance of the compound from the plasma, is adequately described by a three-exponential model. Similarly, the total tissue volume of distribution is a well defined outcome measure.

The identifiability and physiological meaning of the rate constants can be improved by constraining the regression process to values obtained in a region devoid of receptors (*16,44,53*). K_1, k_2 or their ratio can be derived from these regions and used in fitting receptor-rich regions. This strategy could not be implemented with [^{123}I]iomazenil due to the absence of a region devoid of receptors. Flumazenil displacement (n = 3) clearly showed that 60% of the activity measured in the pons was displaceable. This displace-

TABLE 3
Equilibrium Analysis of Bolus Plus Constant Infusion Experiments

	Frontal	Occipital	Temporal	Striatum	Thalamus	Cerebellum	Pons
Bolus plus constant infusions (n = 5)							
V_T	209.00	267.00	235	125	138	143	60
± s.d.	28.00	32.00	39	10	28	34	19
Bolus plus constant infusion plus flumazenil displacement (n = 3)							
V_T	234.00	281.00	266	127	152	170	63
± s.d.	35.00	53	55	23	25	35	27
V_2	31.00	34	33	23	23	27	23
± s.d.	5.00	5	1	3	4	1	4
f_2	0.032	0.030	0.030	0.043	0.044	0.037	0.043
± s.d.	0.005	0.004	0.001	0.006	0.008	0.002	0.007
BP	20300	248	232	103	129	143	39
± s.d.	38.00	53	56	20	29	36	24
% NSB	14.00	12	13	19	16	16	40
± s.d.	4.00	3	3	1	6	5	10

V_T = total tissue equilibrium volume of distribution; V_2 = nondisplaceable equilibrium volume of distribution; f_2 = free fraction in the nondisplaceable compartment; BP = binding potential as derived from equilibrium analysis; and % NSB = percent nonspecific binding.

able activity could be due to contamination by activity originating in surrounding regions, due to the limited resolution of the SPECT device. However, the presence of specific binding in the pons has previously been reported with in vitro studies in the human brain (*50,51*). Our data are consistent with these reports and clearly suggest that the use of the pons as reference region is questionable.

In cortical regions, the nondisplaceable binding represented only 13% of the total binding. The total equilibrium volume of distribution is thus primarily affected by receptor density. Koeppe et al. (*16*) proposed a two-compartment model for the analysis of [^{11}C]flumazenil PET data, with tissue distribution volume (including both specific and nonspecific binding) as outcome measure. The kinetic method proposed here is equivalent to this solution in the sense that the total volume of distribution is the outcome measure.

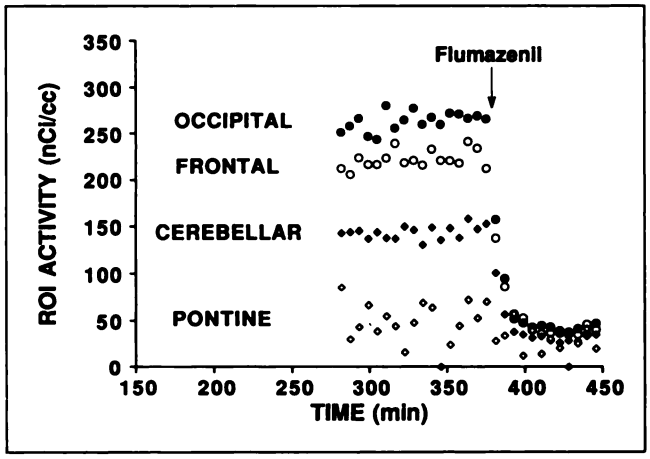

FIGURE 6. Regional ROI time-activity curves from a constant infusion experiment followed by flumazenil displacement in a 24-yr-old female. Scanning started at 280 min and ended at 450 min. Injection of flumazenil (0.2 mg/kg) resulted in 84% displacement in the occipital, 82% in the frontal, 78% in cerebellar and 50% in pontine ROIs. Specific binding was measured directly by subtracting the nonspecific from the total activity. The ratio of the specific binding to the free, measured in plasma over the last 2 hr, gave BP values of 199, 163, 102 and 22 in the occipital cortex, frontal cortex, cerebellum and pons, respectively.

A constant infusion plus flumazenil displacement paradigm was developed to provide direct measurements of regional V_2. V_T values as measured during constant infusion were close to V_T values derived from kinetic analysis. This method presents several advantages over the kinetic method:

1. Direct measurement of V_2 by flumazenil injection. This displacement method was developed because of the difficulties associated with the proper derivation of V_2 by the kinetic method.
2. Direct measure of the free tracer. The prolonged plasma steady-state allows the free tracer to equilibrate on both sides of the BBB. The validity of this method has been demonstrated in rodents and baboons with CSF measurements (*32,35*) and microdialysis (*54*).
3. Computational simplicity. The outcome measure is obtained by a simple ratio. This would allow an easy implementation of a pixel-by-pixel representation of BP.
4. Prolonged acquisition time. At equilibrium, the activity level being stable, the image acquisition time can be increased. Thus, this method appears to be well suited to SPECT, which has a lower sensitivity than PET.
5. Reduced scanning time. For proper derivation of V_T with the kinetic method, the subject has to stay in the camera for 100–120 min. With the equilibrium paradigm, this time can be reduced to 60 min because only one acquisition before and one after flumazenil injection is needed.

6. No arterial sampling. At steady-state, the arterial and venous plasma concentrations equilibrate, allowing the measurement of tracer C_{SS} concentration from one venous blood sample, which further facilitates the experimental procedure.

Several disadvantages of the constant infusion technique must be noted. Although scanning time is reduced, the total experimental time is increased from 120 min to 500 min. There is a potential for pump failure and finally, if subject peripheral clearance is extremely fast or slow, equilibrium may not be reached by the time of scan acquisition.

Low specific activity [^{123}I]iomazenil constant infusion experiments were used in primates to derive in vivo [^{123}I]iomazenil K_D and B_{max} (*33,35*). Derivation of these parameters with kinetic analysis is complex since the model becomes nonlinear at significant levels of receptor occupancy. In contrast, Scatchard analysis can easily be performed on equilibrium data. We are in the process of extending these low specific activity experiments to humans.

Assuming an in vivo K_D of 0.59 n*M* (value measured in primates with low specific activity SPECT experiments) (*33*), the occipital BP value of 244 reported here would correspond to a B_{max} of 141 n*M*. This value is close to the B_{max} measured in vitro in 12 subjects (B_{max} of 162 ± 52 n*M*). In vitro and in vivo values were thus consistent.

In conclusion, both kinetic and equilibrium methods provide adequate measures of regional total equilibrium distribution volume of [^{123}I]iomazenil. Following establishment of equilibrium tracer conditions, the injection of receptor-saturating doses of flumazenil directly measures the equilibrium distribution volume of the nonspecific compartment. The reproducibility of each method is currently being tested.

In comparison to PET, quantitation of SPECT activity is less well developed and more vulnerable to scatter and attenuation. In light of these limitations, the SPECT results reported here compare favorably with PET measurements of benzodiazepine receptors in terms of absolute values and identifiability of parameters. The decreased cost and wider availability of SPECT technology may facilitate the application of these research methods to clinical studies.

ACKNOWLEDGMENTS

The authors thank Walter Hunkeler, PhD (Hoffman-La Roche, Basel, Switzerland) for providing samples of flumazenil and iomazenil; E.O. Smith, G. Wisniewski and Quinn Ramsby for their excellent technical assistance in collecting and analyzing the in vivo data; and S. Giddings for performing the in vitro experiments.

REFERENCES

1. Roy A, Bakay E, Harris A. Neurotransmitter, receptor and biochemical changes in monkey cortical epileptic foci. *Brain Res* 1980;206:387–404.
2. Savic I, Roland P, Sedvall G, Persson A, Pauli S, Widen L. In vivo demonstration of reduced benzodiazepine receptor binding in human epileptic foci. *Lancet* 1988;2:863–866.
3. Johnson EW, de Lanerolle NC, Kim JH, et al. "Central" and "peripheral" benzodiazepine receptors: opposite changes in human epileptogenic tissue. *Neurology* 1992;42:811–815.
4. Owen F, Poulter M, Waddington JL, Mashal RD, Crow TJ. [^{3}H]Ro 05-4864 and [^{3}H]flunitrazepam binding in kainate-lesioned rat striatum and temporal cortex of brains from patients with senile dementia of the Alzheimer type. *Brain Res* 1983;278:373–375.
5. Shimohama S, Taniguchi T, Fujiwara M, Kameyama M. Change in benzodiazepine receptors in Alzheimer type dementia. *Ann Neurol* 1988;23:404–406.
6. Penney JB, Young AB. Quantitative autoradiography of neurotransmitter receptors in Huntington disease. *Neurology* 1982;32:1391–1395.
7. Walker FO, Young AB, Penney JB, Dovorini-Zis K, Shoulson I. Benzodiazepine and GABA receptors in early Huntington's disease. *Neurology* 1984;34:1237–1240.
8. Whitehouse PJ, Trifiletti RR, Jones BE, et al. Neurotransmitter receptor alterations in Huntington's disease: autoradiographic and homogenate studies with special reference to benzodiazepine receptor complexes. *Ann Neurol* 1985;18:202–210.
9. Kiuchi Y, Kobayashi T, Takeuchi J, Shimizu H, Ogata H, Toru M. Benzodiazepine receptors increase in postmortem brain of chronic schizophrenics. *Eur Arch Psych Neurol Sci* 1989;239:71–78.
10. Benes FM, Vincent SL, Alsterberg G, Bird ED, SanGiovanni JP. Increased GABAa receptor binding in superficial layers of cingulate cortex in schizophrenics. *J Neurosci* 1992;12:924–929.
11. Squires RF, Lajtha A, Saesderup E, Palkovits M. Reduced [^{3}H]flunitrazepam binding in cingulate cortex and hippocampus of postmortem schizophrenic brains: is selective loss of glutamatergic neurons associated with major psychoses? *Neurochem Res* 1993;18:219–223.
12. Hantraye P, Kaijima M, Prenant C, et al. Central type benzodiazepine binding sites: a position emission tomography study in the baboon's brain. *Neurosci Lett* 1984;48:115–120.
13. Samson Y, Hantraye P, Baron JC, Soussaline F, Comar D, Maziere M. Kinetics and displacement of [^{11}C] Ro 15-1788, a benzodiazepine antagonist, studied in human brain in vivo by positron tomography. *Eur J Pharmacol* 1985;110:247–251.
14. Persson A, Ehling E, Erikson L, et al. Imaging of [^{11}C]-labeled Ro 15-1788 to benzodiazepine receptors in the human brain by positron emission tomography. *J Psychiat Res* 1985;19:609–622.
15. Shinotoh H, Yamasaki T, Inoue O, et al. Visualization of specific binding sites of benzodiazepine in human brain. *J Nucl Med* 1986;27:1593–1599.
16. Koeppe RA, Holthoff VA, Frey KA, Kilbourn MR, Kuhl DE. Compartmental analysis of [^{11}C]flumazenil kinetics for the estimation of ligand transport rate and receptor distribution using positron emission tomography. *J Cereb Blood Flow Metab* 1991;11:735–744.
17. Beer H-F, Blauenstein PA, Hasler PH, et al. In vitro and in vivo evaluation of iodine-123 Ro 16-0154: a new imaging agent for SPECT investigations of benzodiazepine receptors. *J Nucl Med* 1990;31:1007–1014.
18. Innis R, Zoghbi S, Johnson E, et al. SPECT imaging of the benzodiazepine receptor in non-human primate brain with [^{123}I]Ro 16-0154. *Eur J Pharmacol* 1991;193:249–252.
19. Woods SW, Seibyl JP, Goddard AW, et al. Dynamic SPECT imaging after injection of the benzodiazepine receptor ligand [^{123}I]iomazenil in healthy human subjects. *Psychiatry Res Neuroimaging* 1992;45:67–77.
20. Carson RE. Precision and accuracy considerations of physiological quantification in PET. *J Cereb Blood Flow Metab* 1991;11:A45–A50.
21. Mintun MA, Raichle ME, Kilbourn MR, Wooten GF, Welch MJ. A quantitative model for the in vivo assessment of drug binding sites with positron emission tomography. *Ann Neurol* 1984;15:217–227.
22. Farde L, Hall H, Ehrin E, Sedvall G. Quantitative analysis of D2 dopamine receptor binding in the living human brain by PET. *Science* 1986;231:258–261.
23. Holthoff VA, Koeppe RA, Frey KA, Kilbourn MR, Kuhl DE. Differentiation of radioligand delivery and binding in the brain: validation of a two-compartment model for [^{11}C]flumazenil. *J Cereb Blood Flow Metab* 1991; 11:745–752.
24. Price JC, Mayberg HS, Dannals RF, et al. Measurement of benzodiazepine receptor number and affinity in humans using tracer kinetic modeling, positron emission tomography, and [^{11}C]-flumazenil. *J Cereb Blood Flow Metab* 1993:13:656–667.
25. Iyo M, Itoh T, Yamasaki T, et al. Quantitative in vivo analysis of benzodiazepine binding sites in the human brain using positron emission tomography. *Neuropharmacology* 1991;30:207–215.
26. Pauli S, Liljequist S, Farde L, et al. PET analysis of alcohol with the brain disposition of [^{11}C]flumazenil. *Psychopharmacol* 1992;107:180–185.
27. Pappata S, Samson Y, Chavoix C, Prenant C, Maziere M, Baron JC.

Regional specific binding of [^{11}C]Ro 15-1788 to central type benzodiazepine receptors in human brain: quantitative evaluation by PET. *J Cereb Blood Flow Metab* 1988;8:304–313.
28. Litton J-E, Neiman J, Pauli S, et al. PET analysis of [11C]flumazenil binding to benzodiazepine receptors in chronic alcohol-dependent men and healthy controls. *Psychiatry Res Neuroimaging* 1992;50:1–13.
29. Brouillet E, Chavoix C, Khalili-Varasten M, et al. Quantitative evaluation of benzodiazepine receptors in live Pappio Anubis baboons using positron emission tomography. *Mol Pharmacol* 1990;38:445–451.
30. Carson RE, Channing MA, Blasberg RG, et al. Comparison of bolus and infusion methods for receptor quantification: application to [^{18}F]-cyclofoxy and positron emission tomography. *J Cereb Blood Flow Metab* 1992;13:24–42.
31. Frey KA, Ehrenkaufer LE, Beaucage S, Agranoff BW. Quantitative in vivo receptor binding I. Theory and application to the muscarinic cholinergic receptor. *J Neurosci* 1985;5:421–428.
32. Kawai R, Carson RE, Dunn B, Newman AH, Rice KC, Blasberg RG. Regional brain measurement of B_{max} and K_D with the opiate antagonist cyclofoxy: equilibrium studies in the conscious rat. *J Cereb Blood Flow Metab* 1991;11:529–544.
33. Laruelle M, Abi-Dargham A, Rattner Z, et al. SPECT measurement of benzodiazepine receptor number and affinity in primate brain: a constant infusion paradigm with [^{123}I]iomazenil. *Eur J Pharmacol* 1993;230:119–123.
34. Laruelle M, Baldwin RM, Rattner Z, et al. SPECT quantification of [^{123}I]iomazenil binding to benzodiazepine receptors in nonhuman primates. I. Kinetic modeling of single bolus experiments. *J Cereb Blood Flow Metab* 1994: in press.
35. Laruelle M, Abi-Dargham A, Al-Tikriti MS, et al. SPECT quantification of [^{123}I]iomazenil binding to benzodiazepine receptors in nonhuman primates. II. Equilibrium analysis of constant infusion experiments and correlation with in vitro parameters. *J Cereb Blood Flow Metab* 1994: in press.
36. Zea-Ponce Y, Baldwin R, Zoghbi SS, Innis RB. Formation of 1-[^{123}I]iodobutane in iododestannylation with [^{123}I]iomazenil: implication for the reaction mechanism. *Int J Appl Radiat Isot* 1993;45:63–68.
37. McBride BJ, Baldwin RM, Kerr JM, Wu JL. A simple method for the preparation of ^{123}I- and ^{125}I-labeled iodobenzodiazepines. *Appl Radiat Isot* 1991;42:173–175.
38. Holman BL, Carvalho PA, Zimmerman RE, et al. Brain perfusion SPECT using an annular single crystal camera: initial clinical experience. *J Nucl Med* 1990;31:1456–1461.
39. Zubal IG, Harrell C, Woods SW, et al. Comparison of quantitation linearity of three brain SPECT imaging instruments using ^{99m}Tc and ^{123}I. *J Nucl Med* 1990;31:769–770.
40. Innis RB, Al-Tikriti MS, Zoghbi SS, et al. SPECT imaging of the benzodiazepine receptor: feasibility of in vivo potency measurements from stepwise displacement curves. *J Nucl Med* 1991;32:1654–1761.
41. Malison RT, Miller EG, Greene R, Hoffer PB, McCarthy G, Innis RB. Computer-assisted coregistration of multislice SPECT and MRI images by fixed external fiducials. *J Comp Assist Tomogr* 1992;17:952–960.
42. Zoghbi SS, Baldwin RM, Seibyl JP, et al. Pharmacokinetics of the SPECT benzodiazepine receptor radioligand [^{123}I]iomazenil in human and nonhuman primates. *Nucl Med Biol* 1992;19:881–888.
43. Phelps ME, Huang SC, Hoffman EJ, Selin C, Sokoloff L, Kuhl DE. Tomographic measurement of local cerebral glucose metabolic rate in humans with (F-18)2-fluoro-2-deoxy-D-glucose: validation of method. *Ann Neurol* 1979;6:371–382.
44. Frost JJ, Douglass KH, Mayberg HS, et al. Multicompartimental analysis of ^{11}C-carfentanil binding to opiate receptors in human measured by positron emission tomography. *J Cereb Blood Flow Metab* 1989;9:398–409.
45. Levenberg K. A method for the solution of certain problems in least squares. *Quart Appl Math* 1944;2:164–168.
46. Landlaw EM, DiStefano JJ III. Multiexponential, multicompartmental, and noncompartmental modeling. II. Data analysis and statistical considerations. *Am J Physiol* 1984;246:R665–R677.
47. Akaike H. A new look at the statistical model identification. *IEEE Trans Automat Contr* 1974;AC19:716–723.
48. Carson RE. Parameters estimation in positron emission tomography. In: Phelps ME, Mazziotta JC, Schelbert HR, eds. *Positron emission tomography. Principles and applications for the brain and the heart*. New York: Raven Press; 1986;347–390.
49. Munson P, Rodbard D. LIGAND: a versatile computerized approach for characterization of ligand binding systems. *Ann Biochem* 1980;107:220–239.
50. Mohler H, Okada T. Benzodiazepine receptor: demonstration in the central nervous system. *Science* 1977;198:849–851.
51. Braestrup C, Albrechten R, Squires RF. High densities of benzodiazepine receptors in human cortical areas. *Nature* 1977;269:702–704.
52. Maloteaux JM, Luabeya MAK, Vanisberg MA, et al. Benzodiazepine receptors in normal human brain, in Parkinson's disease and in progressive supranuclear palsy. *Brain Res* 1988;446:321–332.
53. Farde L, Eriksson L, Blomquist G, Halldin C. Kinetic analysis of central [^{11}C]raclopride binding to D_2 dopamine receptors studied by PET—A comparison to the equilibrium analysis. *J Cereb Blood Flow Metab* 1989;9:696–708.
54. Dubey RK, McAllister CB, Inoue M, Wilkinson GR. Plasma binding and transport of diazepam across the blood-brain barrier. No evidence for in vivo enhanced dissociation. *J Clin Invest* 1989;84:1155–1159.